Proceedings, 7th African Rift Geothermal Conference
Kigali, Rwanda 31st October – 2nd November 2018

Focused Inversion of Gravimetric and Magnetotelluric Data for Geothermal Investigations

Egidio Armadillo[1], Daniele Rizzello[2], Claudio Pasqua[3], Paolo Pisani[3], Alessandro Ghirotto[1], Taramaeli Mnjokava[4], Jonas Mwano[4], Makoye Didas[4], Lucas Tumbu[4]

1) DISTAV, Universita' di Genova, Italy 2) Tellus s.a.s., Italy 3) ELC-Electroconsult, Italy 4) Tanzania Geothermal Development Company Ltd (TGDC), Tanzania

egidio@dipteris.unige.it; geodriz75@yahoo.it, claudio.pasqua@elc-electroconsult.com; paolo.pisani@elc-electroconsult.com; ale.ghir8@gmail.com; taramaeli.mnjokava@tanesco.co; jonas.mwano@tanesco.co.tz; didas.makoye@tanesco.co.tz; lucas.tumbu@tanesco.co.tz

Keywords

Magnetotelluric, Gravimetry, Focused inversion, Luhoi

ABSTRACT

Focused inversion techniques may be applied to geophysical data inversion in order to image complex structures in the subsoil. These algorithms may image complex "blocky" structures giving useful information in geothermal exploration that may be smoothed out by standard inversion algorithms that use stabilizer that penalize sharp transitions.

We have tested the modified total variation and the maximum gradient support stabilizers in the inversion of synthetic and field magnetotelluric and gravimetric data. The gravimetric data from the Luhoi geothermal prospect have been used to map the sharp density transition between the sandstone and the overlying claystone layers. The resulting horst structure imaged in 2D and 3D models by the maximum gradient support stabilizer solution allow to trace the main fault system that drives the up-flow of hydrothermal waters. The 1D magnetotelluric "blocky" models with lateral constrain (pseudo-3D) image the lithological contact between the claystone and sandstone far from the horst area and reveal resistivity variations in the claystone layer associated with sand lenses. In the horst area, resistivity models image hydrothermal alteration affecting the sandstone layer.

1. Introduction

Geophysical surveys are considered indispensable tools in geothermal exploration to image buried tectonic structures and variations of lithology, hydrothermal alteration type and porosity/fluid content. The final geophysical products are inverse models that can be directly used for the assessment of the geothermal conceptual model. Typical inverse models use Tikhonov (Tikhonov and Arsenin, 1977) zero order (minimum norm of the solution) or first

order (minimum norm of the solution first derivative) regularization techniques (e.g. Zhdanov, 2002). For instance, in the Occam inversion algorithm (Constable et al., 1987) the smoothest model that fits the data to within an expected tolerance is sought using the first order Tikhonov regularization. Due to the adopted regularization approach, the resulting images usually are smooth models and penalize sharp transitions. While this approach prevents over-interpretation of the data, in some cases important abrupt changes of the geophysical parameters may be smoothed out and missed. Typical examples are the lithological variations between the sedimentary infill and the bedrock in a basin or the bedrock steps due to faulting in graben/horst structures.

Focused geophysical imaging with different regularization methods can be effective to detect sharp boundaries allowing to map buried faulting in the bedrock and lithological variations. For instance, the total variation regularization function (Rudin et al., 1992) and its modifications (Vogel and Oman, 1998) can be effective when moderate discontinuous jumps in the model are expected. Another alternative is the minimum gradient support functional (Portniaguine and Zhdanov, 1999) that minimizes the area where strong model parameter variations and discontinuity occur and therefore helps to generate a stable solution of the inverse problem for complex geological environment that are better modelled by blocky rather than smooth structures.

These methods aren't commonly used for geophysical investigations, and no example from geothermal exploration is known to us. Here we evaluate their effectiveness and practicality. We have applied these focused regularization techniques to the gravimetric and magnetotelluric data set collected over the geothermal field of Luhoi, in Tanzania (Armadillo et al., this volume). In the following we discuss the results and show major advantages and drawbacks.

2. Methodology

A typical non-linear forward problem can be described by the relationship (e.g. Zhdanov, 2002):

$$d = G(m)$$

where m are the model parameters, d the geophysical observations and G the forward operator.

The inverse problem consists in estimate m from d. This problem is usually ill-posed since the solution can be non-unique and unstable (e.g. Zhdanov, 2002). Ill-posed inverse problems are generally solved looking for the model m that minimizes the Tikhonov parametric functional (Tikhonov and Arsenin, 1977):

$$T(m) = f(m) + \alpha\, s(m)$$

The misfit functional $f(m)$ measures the fit between the observed data d_o and the predicted data $d=G(m)$ by the current model m. Usually the fit $f(m)$ is computed as the squared norm of the differences between observed and predicted data scaled by the errors σ:

$$f(m) = \left\| \frac{d_o - G(m)}{\sigma} \right\|^2$$

The term s*(m)* is a stabilizing functional that measures the distance of the current model *m* from a model with some sought characteristic and it is discussed in the following.

The parameter α is the regularization parameter that weights the contribution to *T(m)* of the two functionals *f(m)* and *s(m)*.

One of the most common choice for the stabilizer *s(m)* is the maximum smoothness stabilizing functional (MS) that operates on the gradient $\nabla m(r)$ of the model parameters *m:*

$$s(m) = \int_V |\nabla m(r)|^2 \, dv$$

This functional minimizes the difference between adjacent parameters *m* and produces smooth models that contain the minimum structure necessary to predict the measured data d_o. A typical algorithm using this functional is the Occam inversion scheme introduced by Constable et al. (1987) and is applied to many different geophysical problems.

To improve focusing of the solution, Acar and Vogel (1994) introduced the modified total variation stabilizing functional (modTV):

$$s(m) = \int_V \sqrt{|\nabla m(r)|^2 + \beta^2} \, dv$$

This functional does not penalize discontinuity in the model parameters *m* and allow for piecewise smooth solutions (Vogel and Oman, 1998). The penalties are applied to gradient terms much larger than β while gradient terms much smaller than β are penalized. For this reason, the resulting models maybe still too smooth to image complex blocky structures.

To reduce the smoothness effect of modTV, Portniaguine and Zhdanov (1999) introduced the minimum gradient support functional (MGS) that would minimize the area where significant variations of the model parameters and/or discontinuity occur:

$$s(m) = \int_V \frac{\nabla m \cdot \nabla m}{\nabla m \cdot \nabla m + \beta^2} dv$$

For a given value of β, the gradient terms that are much less than β have a very small contribution on the total value of *s(m)*, while terms much larger than β have all contributions equal to one and therefore large gradient are not penalised. With this functional, solutions with sharp boundaries are promoted and the penalty for large gradients is reduced (Portniaguine and Zhdanov, 1999).

We have implemented the three functionals in magnetotellurics (MT) and gravimetric data inversion algorithms in the MatLab environment. For the gravity forward modelling routine, we have used the formula for 3D prismatic bodies of Banerjee and Das Gupta (1977). For the 1D MT forward routine we have used the classical iterative formula (e.g. Zhdanov and Keller, 1996). The optimization algorithm is based on the Sequential Quadratic Programming (SQP) method (e.g. Nocedal and Wright, 2006) for non-linear inversion problems.

3. Synthetic tests

We have first compared the performances of the three functionals MS, modTV and MGS both on the gravimetric data generated from a 2D synthetic model (Fig. 1) and on the magnetotelluric data from a 1D synthetic model (Fig. 2).

The density model for gravity (Fig. 1a) simulates an asymmetric blocky horst structure covered by sediments with a density contrast of -0.2 g/cm^3. The horst is composed of five steps labelled S1-S5. The bedrock steps differ each other for their depth and for the length of the planar sector between them. Two "impulsive" sources labelled B1 and B2 are inserted at different depth to test the response of the different functionals to this kind of sources and to qualitatively evaluate the sensitivity of the data at different depth. The gravimetric signal is supposed to be acquired over a flat Earth with 250 m sampling and a random error was applied with zero mean gaussian distribution and standard deviation of 0.05 mGal. All the inversions are performed looking for the maximum value of the regularization parameter α that gives a root means square error of 0.05 mGal. The sedimentary cover has been approximated by prisms of 200 m width, density of -0.2 g/cm^3 and unknown thickness to be estimated.

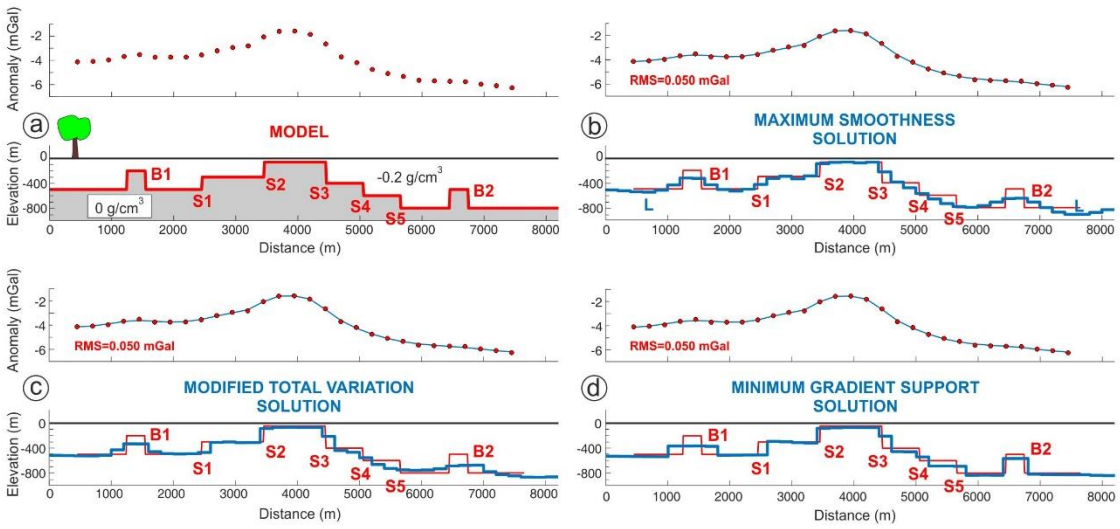

Figure 1: Example of 2D gravimetric data inversion with different stabilizing functional. a) Model simulating a horst structure made by steps (S1 – S5) in the bedrock and overlain by sediments with density contrast of -0.2 g/cm^3. Two 'impulsive' sources B1 and B2 have been added at different depth. b) Final estimated model using the maximum smoothness stabilizing functional MS. The cyan label L indicate spurious oscillations of the bedrock that are typically obtained with this functional where discontinuities occur. c) Final estimated model using the modified total variation functional modTV. d) Final estimated model using the minimum gradient support functional MGS.

The MS functional solution (Fig. 1b) reproduces the shallow bedrock step S2 (range depth 50-300 m). Step S1 (range depth 300-500 m) is smoothed out but the two flat areas around it are well imaged. Steps S3, S4 and S5 (range depth 50-400, 400-600 and 600-800 m respectively) are totally smoothed out. This effect is due both to the increasing depth and to the short distance (600 m) between them. The 'impulsive' sources B1 and B2 are strongly smoothed but they are visible and well centred. Note the spurious oscillations (indicated by

the cyan label L) that appear close to the model discontinuities B that characterize the inverted models by this functional as noted by Portniaguine and Zhdanov (1999).

In the modTV solution (Fig. 1c) steps S1 and S3 are imaged but affected by a small lateral error of the order of the prism length (200 m), that is the minimal model resolution. Steps S4 and S5 are still smoothed out. Imaging of 'impulsive' sources B1 is not improved while B2 is not well resolved.

Finally, the MGS solution (Fig. 1d) shows the best improvement in model resolution. Steps S1 and S3 are still affected by relatively small horizontal and depth errors. Steps S4, S5 and S6 are now imaged, even if with some errors. The deeper 'impulsive' sources B2 is (surprisingly) well resolved while B1 is centred but the lateral dimensions and depth are missed.

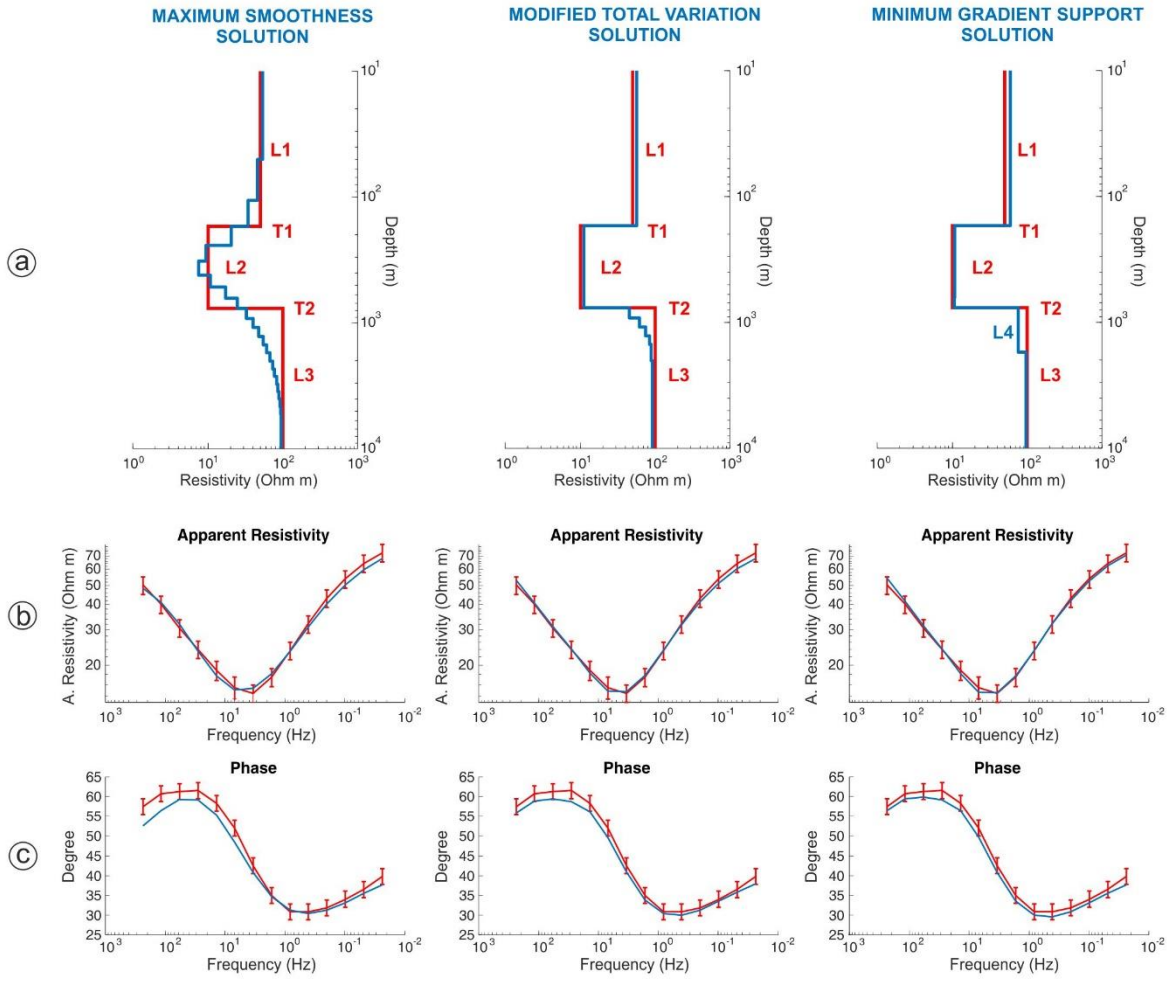

Figure 2: Example of 1D magnetotelluric data inversion with different stabilizing functional. a) The 'true' model (in red) simulates a typical geothermal environment with overburden (L1, thickness 150 m, resistivity 50 Ohm m), clay cap (L2, 650 m, 10 Ohm m) and a resistive substratum (L3, 100 Ohm m). The inverted models resulting from the MS, modTV and MGS functionals are drawn in cyan from left to right respectively. b) Comparison between the synthetic apparent resistivity data (red line) and model response (cyan line) for the three corresponding final models. c) The same for the phase.

The MT resistivity test model is shown in red in Fig. 2a. It simulates a typical three layers geothermal feature, with the middle low resistivity layer L2 (10 Ohm m, depth range 150 - 800 m) associated with the “clay cap” and embedded between an overburden at 50 Ohm m (L1) and a resistive substratum at 100 Ohm m (L3). Synthetic data were contaminated by 5% gaussian noise. The inverted models obtained by the three different functionals MS, modTV and MGS are shown in cyan. In Fig. 2b and 2c the model response and data fit are shown. The three models have a comparable misfit.

The MS solution smooths out the sharp transitions T1 and T2 of the model. Smoothing is stronger at the deepest transition T2 (note the logarithmic depth scale). Recovery of the depth of the sharp boundaries is impossible. The modTV solution shows an impressive improvement in the imaging of the shallower boundary T1 while the deepest T2 is still lightly smoothed out. The MGS shows the best resolution. T1 transition is well resolved; T2 transition is correctly imaged but a spurious layer L4 is introduced with a light variation from the third 'true' layer L3.

4. Gravimetric and magnetotelluric 2d focused models of the Luhoi prospect

We have evaluated the effectiveness of the MGS stabilizer to recover the structure and lithological variations of the Luhoi geothermal prospect in Tanzania.

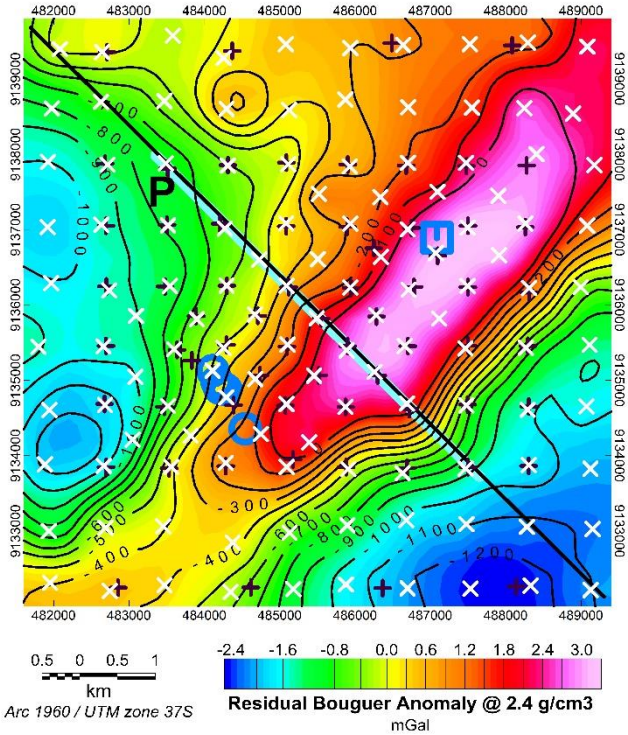

Figure 3: Residual Bouguer anomaly map of the Luhoi geothermal prospect (from Armadillo et al., this volume). Locations of the gravimetric and magnetotelluric stations are marked by white and black crosses respectively. The contour represents the elevation of the claystone-sandstone contact obtained by 3D smooth gravity inversion and images the NE trending horst structure. The Nyongoni springs and the Wingoyongo well are marked by cyan circles and square respectively. The black line is the trace of the profile P shown in Fig. 4, 5 and 6; the portion of the profile covered by the MT stations is marked in light blue.

Here a horst structure trending NE has been imaged by MT and gravimetric modelling (Armadillo et al., this volume). The fluid up-flow has been interpreted to be driven by the horst normal faults and therefore hydrothermal alteration is expected to be confined in the horst area. The location of the measurement stations and the gravimetric residual Bouguer anomaly is shown in Fig. 3.

The horst is made by an uplifted block made by sandstones generating the positive NE trending gravimetric anomaly, with younger less dense and less resistive claystones at both sides (Armadillo et al., this volume). In the figure we have also mapped the contour lines of the elevation of the claystone-sandstone contact obtained by the 3D smooth inversion of the whole dataset (Armadillo et al., this volume). A crucial information in such a case is the mapping of the buried normal fault system originating the horst, since they act as preferred fluid path-ways. We have therefore tested the MGS functional on this data set along the 2D section shown as black line in Fig. 3.

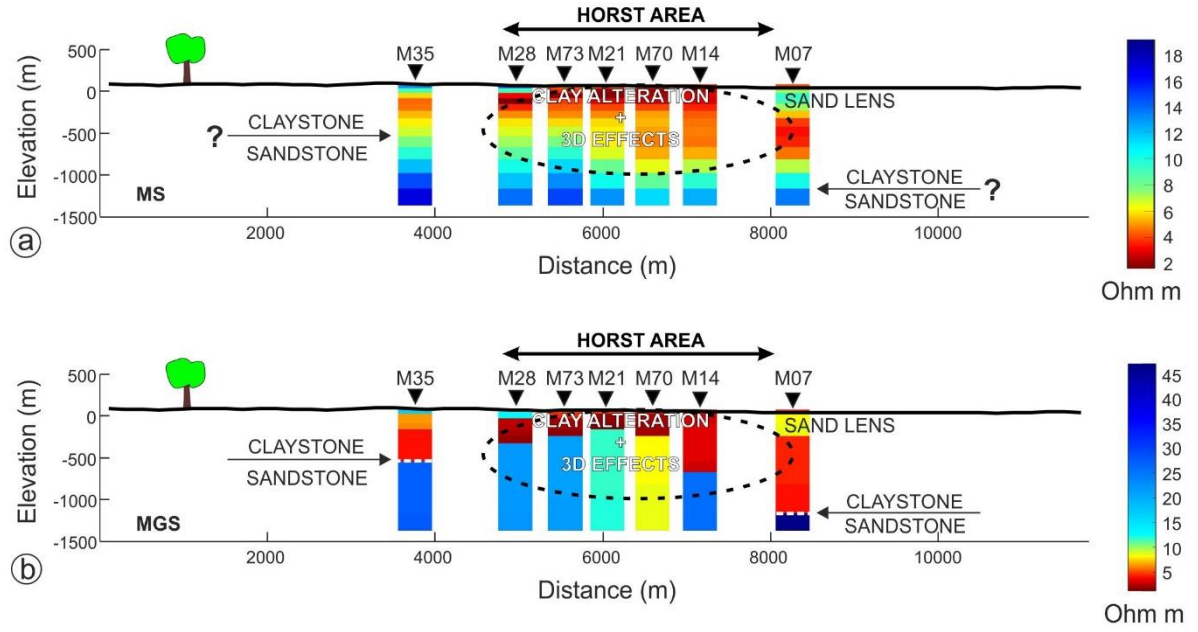

Figure 4: Magnetotelluric pseudo-2D inversion along profile P (no vertical exaggeration). a) Inverted model with the MS functional for both vertical and horizontal regularization. b) The same for the MGS functional. The shallow low resistivity layer is associated with the claystone in the area far from the horst (MT stations M35 and partially M07). However, only the MGS solution b) images the contact between claystone and sandstone (dashed white line). In the horst area hydrothermal clay alterations and 3D effects prevent a pure lithological interpretation of the resistivity. Note the different color scales used for the resistivity in the two panels.

From the magnetotelluric data set we have considered the seven MT stations along the profile and inverted them by a pseudo-2D inversion (1D algorithm with an additional lateral regularization). We inverted the average apparent resistivity and phase data. The resulting electrical resistivity pseudo-2D models obtained by the MS and MGS stabilizing functionals are shown in Fig. 4. The models show a resistive substratum that is overlain by a conductive layer with very variable thickness. Far from the horst area (stations M35 and partially M07) the resistivity is primarily controlled by the lithology and therefore can be used to image the

claystone-sandstone contact (Armadillo et al., this volume). On the contrary, in the horst area, hydrothermal clay alteration and 3D effects are expected to strongly affect the resistivity distribution that cannot therefore be used here to infer the depth of the lithological contact. The superiority of the MGS functional in mapping the sharp lithological transition at stations M35 and M07 is evident (see the white dashed line pointed by the arrows in panel "b"). From the MS solution is not possible to infer the lithological contact (the arrows in panel "a" indicate the contact surface inferred from the MGS solution in panel "b"). Moreover, in the horst area the low resistivity associated with hydrothermal alteration and 3D effects is broader for the MS solution (panel "a"), while the MGS solution (panel "b"), is closer to the true 3D model shown in Armadillo et al. (this volume).

In the case of the gravimetric data set, we have modelled the claystone layer by a set of rectangular prisms of 200 m width, unknown thickness to be estimated and assumed density contrast of -0.16 g/cm^3. We have used as constraint the sandstone top depth resulting from MT station M35 (628 m, Fig. 4). The resulting models from the MS and MGS functionals are shown in Fig. 5 as blue and black lines respectively. From the MGS solution it is possible to image the major faults that define the horst structure (dashed red lines labelled F).

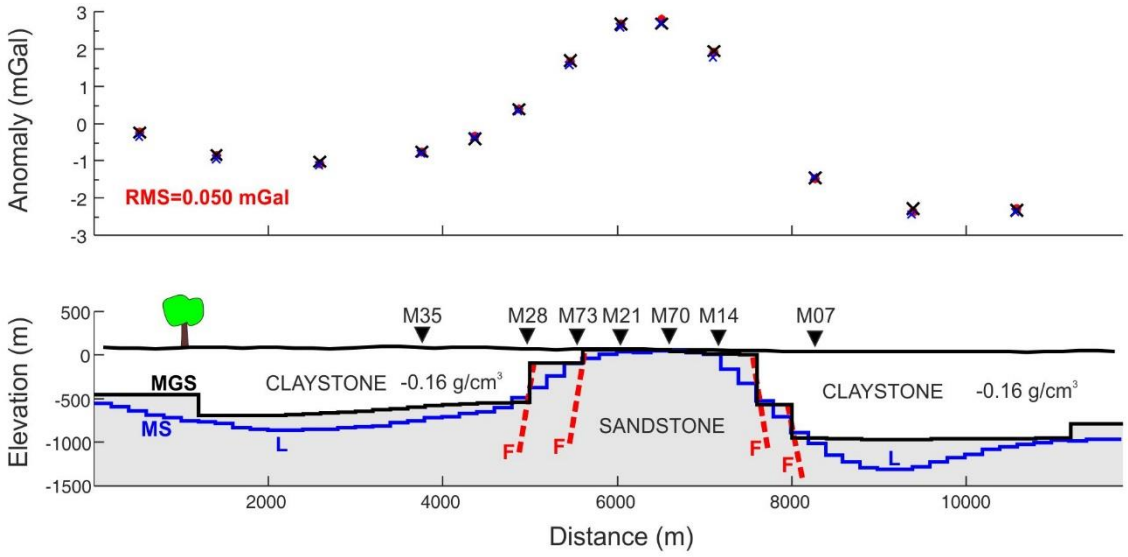

Figure 5: Gravimetric models of the claystone-sandstone interface using the MS and MGS functionals along profile P (no vertical exaggeration). Upper panel: measured data (red circle), MS (blue crosses) and MGS (black crosses) models computed data. Lower panel: comparison between the MS (blue line) and MGS (black line) models. Note the spurious depressions labelled L in the MS model. The MGS model allows the identification of the horst main faults labelled F (dashed black lines).

Finally, we compare the resistivity and density MGS final models in Fig. 6. The density model is constrained by MT station M35 and therefore the match between the gravimetric and MT bottom of the claystone layer here is perfect. In the horst area the mismatch between the claystone distribution and the low resistivity layer is evident. It is due to clay alteration affecting the sandstone (verified at the Wingoyongo well, see Fig. 3 for location) and also to 3D lateral effects that bias 1D modelling. On the other side of the horst at MT station M07

there is a difference ε of about 200 m in the bedrock estimation between the resistivity and density models. This difference may depend on density variations in the claystone due to sandstone lenses, clay alterations in the sandstones and/or 3D bias due to resistivity lateral variations.

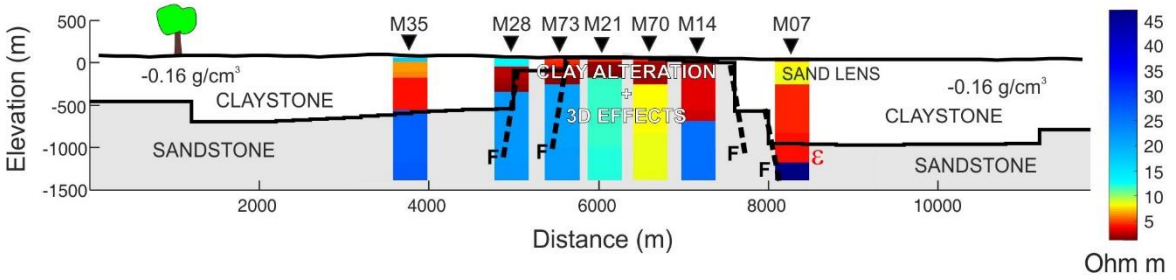

Figure 6: Comparison between density and resistivity MGS models along profile P (no vertical exaggeration applied). The faults F (black dashed lines) are inferred from the horst structure imaged by gravity. At MT station M07 the resistivity contrast due to the claystone-sandstone contact is about ε = 200 m deeper than the imaged density contrast surface.

5. Preliminary gravimetric and magnetotelluric 3d focused models of Luhoi

We have also tested a true 3D gravimetric MGS inversion as well as a pseudo 3D (1D with lateral constrain) magnetotelluric MGS inversion of the Luhoi data set. The inversions are still at a preliminary study stage.

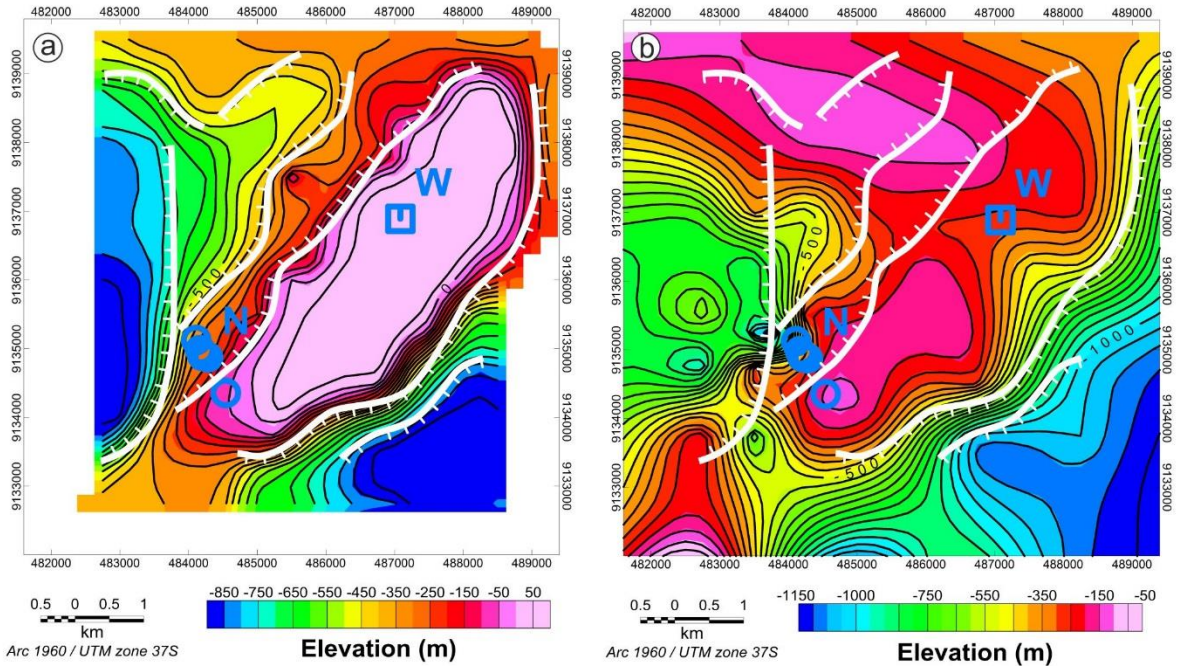

Figure 7: a) Elevation (color scale and contour) of the top of the sandstone layer derived from the 3D MGS gravimetric inversion. The white lines trace the main faults inferred from the maxima of the horizontal gradient of the inverted gravimetric bedrock. b) Elevation (color scale and contour) of the resistive bedrock derived from the pseudo 3D MGS inversion (1D MGS inversion with lateral constrain).

We have applied the MGS inversion to a subset of the gravimetric stations (86 over 124) to reduce the time needed to evaluate the optimal values of α and β parameters (see paragraph 2). A final misfit of 0.3 mGal has been obtained. The elevation of the final density contrast surface is shown as color map in Fig. 7a. The MGS solution is a significative improvement with respect to the MS solution (see bedrock contour lines in Fig. 3), especially along the NW flank of the horst, because shows sharper variations in the horizontal gradient enlightened by the narrower contour lines. We interpret these sharp transitions as the morphological expressions of the main faults (white heavy lines) affecting the study area.

The pseudo 3D magnetotelluric MGS model has been used to map the elevation of the resistivity sharp transition from the shallow conductive layer to the resistive bedrock. The resulting map is shown in Fig. 7b. Far from the horst this surface well represents the claystone-sandstone lithological contact. In the horst area resistivity lithological variations are masked by the stronger resistivity variations due to clay alterations affecting the sandstone.

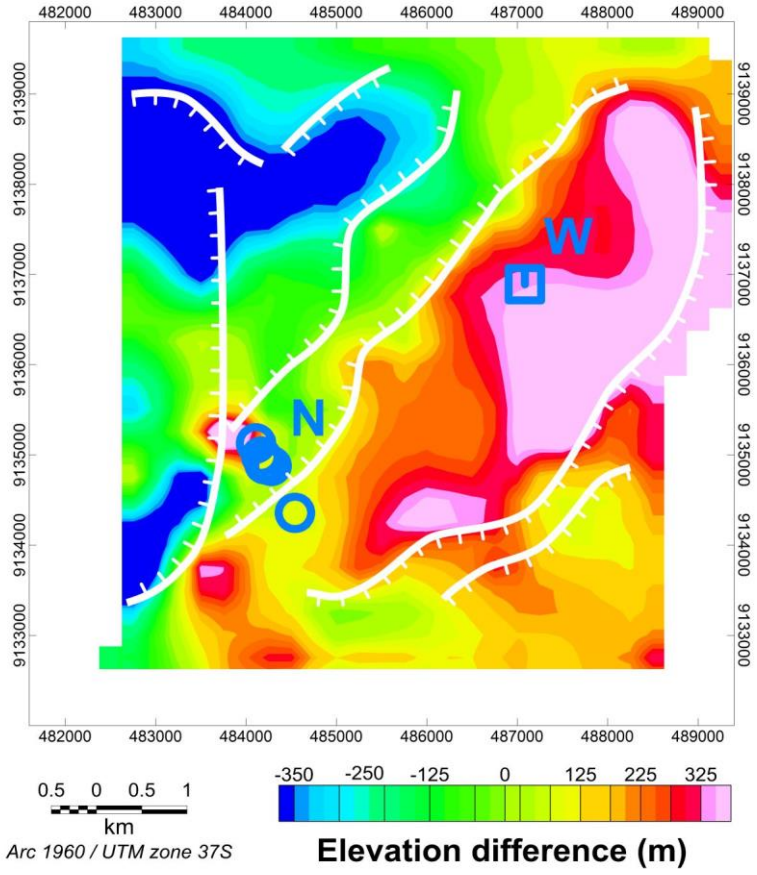

Figure 8: Difference (color map) between the gravimetric and resistive "bedrock. Red-orange colors indicate area where the estimated gravimetric bedrock is above the resistive bedrock. The opposite holds for blue/light blue colors. The white lines are the inferred main faults traced from the main step-like features in the gravimetric bedrock (see Fig. 7a).

We have then computed the difference between the gravimetric and magnetotelluric 'bedrock'. The resultant map is shown in Fig. 8. In the map, red-orange colours indicate areas where the gravimetric bedrock is well above (more than about 200 m) the resistive bedrock. This strong mismatch is likely due to i) alteration in the sandstone that strongly reduces its resistivity and "push down" the resistive bedrock and/or ii) over-estimation of the density contrast between the sandstone and claystone layers (for instance due to sandstone lenses in the claystone) that "push up" the gravimetric bedrock. The anomalous values in the horst area are mainly due to hydrothermal alteration of the sandstones. The anomalous values in the SE sector are likely due to thick denser sandstone lenses in the claystone imaged by MT (see Fig. 4). Blue/light-blue areas indicate areas where the opposite occurs. Note also that the resistivity bedrock estimation may also be biased by 3D effects that the MT 1D forward code cannot account for.

6. Conclusions

We have tested some focused inversion techniques for gravimetric and magnetotelluric inversion in geothermal areas. The work is still at a preliminary stage, however the results are encouraging. Both synthetic and field data tests have shown that focused images may strongly improve interpretation when blocky structures occur.

The field test with the Luhoi data set shows that a more focused image of the lithological contact between sandstone and claystone may be obtained by the use of the MGS functional applied to both gravimetric and magnetotelluric data inversion. Moreover, the gravimetric bedrock obtained by the MGS stabilizer greatly help the tracing of the main faults assuming they correspond to the maxima of the horizontal gradient of the bedrock surface.

Major drawbacks we have found in the use of the MGS stabilizer are i) the longer computational time required for finding the optimal values of α and β parameters (see paragraph 2) to obtain the sought data fit, ii) the necessity of sensitivity testing to evaluate the reliability of the obtained complex structures with respect to the minimum structure solutions obtained with standard smooth inversion procedures, and iii) the strong dependence of the solution upon the initial model chosen.

AKNOWLEDGEMENTS

This work was funded by the Icelandic International Development Agency (ICEIDA) and the Nordic Development Fund (NDF). The Tanzania Geothermal Development Company (TGDC), ELC-Electroconsult S.p.A., Tellus s.a.s. and the Department of Earth, Environment and Life Sciences of the University of Genoa (DISTAV) provided instrumental and technical support.

REFERENCES

Acar, R., and Vogel, C. R. “Analysis of total variation penalty methods” *Inverse Problems*, 10, 1217-1 229 (1994).

Armadillo, E., Rizzello, D., Pasqua, C., Pisani, P., Mnjokava, T., Mwano, J., Didas, M., Tumbu, L.” Geophysical Imaging of the Luhoi Geothermal Field, Tanzania” *this volume.*

Banerjee, B., and Das Gupta, S. P. “Gravitational attraction of a rectangular parallelepiped”. *Geophysics*, 42 (5), 1053-1055 (1977).

Constable, S. C., Parker, R. C., and Constable, G. “Occam's inversion: a practical algorithm for generating smooth models from EM sounding data” *Geophysics*, 52, 289-300 (1987).

Nocedal, J., and Wright, S. J. “Numerical Optimization”, *Second Edition. Springer Series in Operations Research*, Springer Verlag (2006).

Portniaguine, O., and Zhdanov, M. S. “Focusing geophysical inversion images”. *Geophysics*, 64, 3, 874-887 (1999).

Rudin, L. I., Osher, S., and Fatemi, E. “Nonlinear total variation based noise removal algorithms”, *Physica D*, 60, 259-268 (1992).

Tikhonov, A. N., and Arsenin, V. Y. “Solution of ill-posed problems” *V. H, Winston and Sons* (1977).

Vogel, C. R., and Oman, M. E. “Fast total variation based reconstruction of noisy blurred images” *IEEE Trans. Image Processing.*, 7, 813-824 (1998).

Zhdanov, M. S. “Geophysical inverse theory and regularization problems”, *Methods in Geochemistry and Geophysics*, 36, Elsevier (2002).

Zhdanov, M. S., and Keller, G. V. “The Geoelectrical Methods in Geophysical Exploration”. *Elsevier* (1994).